Stepwise retrieval of photosynthesis from reflectance and solar induced fluorescence

MSc Marco Celesti

Remote Sensing of Environmental Dynamics Lab.
Dept. of Earth and Environmental Sciences
University of Milano-Bicocca
m.celesti2@campus.unimib.it

April 25, 2017

COST STSM Reference Number: COST-STSM-ES1309-36163
Period: 2017-02-06 to 2017-04-08
COST Action: ES1309
STSM type: Regular (from Italy to Netherlands)
STSM Topic: Stepwise retrieval of photosynthesis from reflectance and solar induced fluorescence
Host: Dr. Ir. Christiaan van der Tol, University of Twente, Faculty of Geo-Information Science and Earth Observation (ITC), Enschede (NL), c.vandertol@utwente.nl

1 Purpose of this STSM

Sun-Induced chlorophyll fluorescence (F) is a promising tool for monitoring vegetation status from remote. F is an electromagnetic signal emitted in the red and far-red region ($\approx$ 650-800 nm) from plant's photosystems as a dissipative path of the absorbed energy not used for photosynthesis, and it is being increasingly used to retrieve information about vegetation primary productivity and stress from ground-based, airborne and satellite top-of-canopy (TOC) hyperspectral measurements. Although it is strongly linked to vegetation photochemical activity, F is also highly influenced by variation in canopy structure, pigment concentration and environmental conditions (e.g. illumination). According to the recent Global Sensitivity Analysis [1] of the Soil-Canopy Observation of Photochemistry and Energy fluxes (SCOPE) model [2], variables such as incoming radiation, chlorophyll concentration (Cab) and Leaf Area Index (LAI) are major drivers of F intensity. Their variation in the spatial and temporal domain, if not properly accounted for, can lead to biased interpretation of the remotely sensed F signal in relation to the physiological behaviour of the vegetation. To summarize, TOC emitted F can be expressed as a function of leaf and canopy optical properties that drives the fraction of absorbed photosynthetically active radiation (fAPAR) and the reabsorption of the emitted fluorescence, illumination conditions (incident PAR), and plant physiology, that drives the quantum efficiency of fluorescence emission (Φ_F).

The main aim of this STSM was to further investigate the capability of model simulation to complement hyperspectral measurements of vegetation reflectance and fluorescence, in order to retrieve fruitful information on vegetation functioning from above. In particular the STSM was focused on the inversion of several modules of the SCOPE model to retrieve simultaneously vegetation biochemical and biophysical parameters, as well as Φ_F. The retrieved values are the starting point for further modelling vegetation photosynthetic activity, and thus the title of this STSM.

The STSM activity was mainly divided in the following phases:

- data consolidation and preprocessing;
- training on the SCOPE model, and in particular on the RTMo, Fluspect and RTMf modules, as well as on the inversion routine based on MATLAB® `lsqnonlin` function;
- inversion of the coupled RTMo + Fluspect + RTMf radiative transfer model on Top Of Canopy (TOC) high resolution radiance/reflectance measurements collected in the field;
- evaluation of the retrieved parameters and sketch of a synoptic scheme for interpreting vegetation functioning from them.

2 Material and methods

2.1 Measurements setup

The data used in this analysis were acquired from the grant holder and his colleagues in 2014, during a field campaign in Latisana (Udine, Italy), promoted by ESA in the framework of the future FLEX-S3 tandem mission. Six plots of a commercially produced lawn carpet were treated with different doses of a herbicide that interferes with the light reactions of photosynthesis (Chlorotoluron), three additional plots were not treated and used as control. Chlorotoluron inhibits photosynthesis blocking the electron transport chain after the photosystem two (PSII) at the level of Plasto-Quinone (PQ), and is known also to inhibit the Non-Photochemical Quenching (NPQ) of fluorescence. Considering that both PQ and NPQ are blocked or strongly limited, F is expected to increase dramatically in order to dissipate as much energy as possible.

High spectral resolution TOC radiance measurements were collected on each plot with portable spectrometers to compute reflectance and to retrieve F by using advanced Spectral Fitting Methods (SFM, [3]). Nearly simultaneous measurements of canopy-level gas exchange were performed with special closed chambers, and destructive samples were collected for measuring pigments content in laboratory.

Incident (L_{in}) and canopy leaving radiance (L_{out}) were measured in the field with three portable spectrometers operating in the visible and near infrared regions with different spectral resolutions(Table 1).The spectrometers were housed in a Peltier thermally regulated box

Table 1: Summary of the characteristics of the spectrometers used in the measurement campaign. "Pix. num." is the number of pixels in the detector array, "R." is the spectral range, "SSI" is the Spectral Sampling Interval, "FWHM" is the "Full Width at Half Maximum" and "SNR" is the nominal Signal-to-Noise Ratio.

Model	Pix. num.	R. [nm]	SSI [nm]	FWHM [nm]	SNR
HR4000f	3842	400-1000	0.24	1.00	300:1
QE65000	1044	657-743	0.10	0.25	1000:1
HR4000a	4400	717-805	0.02	0.10	300:1

(model NT-16, Magapor, Zaragoza, Spain) keeping the internal temperature at 25C in order to ensure the stability of both the intensity and the spectral information of the measured signal. The targets were measured from nadir with bare optical fibers (field of view of 25) at a distance of 130 cm, yielding to an observed circular surface of approximately 58 cm of diameter. The fibers were mounted downlooking on a specially modified tripod that allowed the alternate measurements of the vegetated target and of the white reference calibrated panel (Labsphere Inc., North Sutton, NH, USA). This system has been widely used in the last decade to provide consistent values of reflectance and fluorescence in different conditions, over a wide range of crops and natural vegetation [4].

Ground measurements were performed over a total time window of approximately one month (between June and July 2014), approximately from 10:00 AM to 16:00 PM depending on the weather conditions. Spectral data were acquired with a dedicated software (3S; [5]) and processed with a specifically developed IDL (ITTVIS IDL 7.1.1) application described in [6], but in this case the dark current was measured over the full spectral range. Each acquisition consisted of three spectra acquired sequentially: incoming radiance (L_{in}), outgoing radiance (L_{out}) and L_{in} again. Relative variation of the two L_{in} measurements was used as a quality check for illumination condition stability. Each of these spectra is the average of 10 and 3 scans (for the full range and the other two spectrometers, respectively) in order to reduce instrumental noise. Plots were measured moving the MSS from P1 to P12 cyclically during the day. Five consecutive acquisitions were taken for each plot under stable illumination conditions before moving to the next one. After quality check and filtering, the final spectral dataset consisted of 1400 measurements.

Figure 1 shows a picture from above of a parcel of the lawn carpet. The white frame is the collar used for gas exchange measurements, it was used as a reference to ensure spatially consistent measurements of the same surface (depicted approximately with the yellow circle) over time. To ensure that the white frame had no effect on the measurements (i.e. adjacency effects) two consecutive measurements with and without the frame were compared, showing no significant differences in terms of reflectance and fluorescence.

The spectra collected with the three spectrometers were merged together in order to obtain the highest possible resolution (Figure 2).

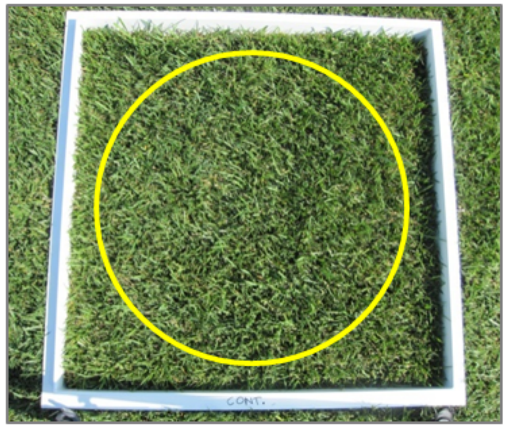

Figure 1: Parcel of the measured lawn carpet. The white frame is the collar used for gas exchange measurements, the yellow circle is approximately the area measured with the spectroscopic system.

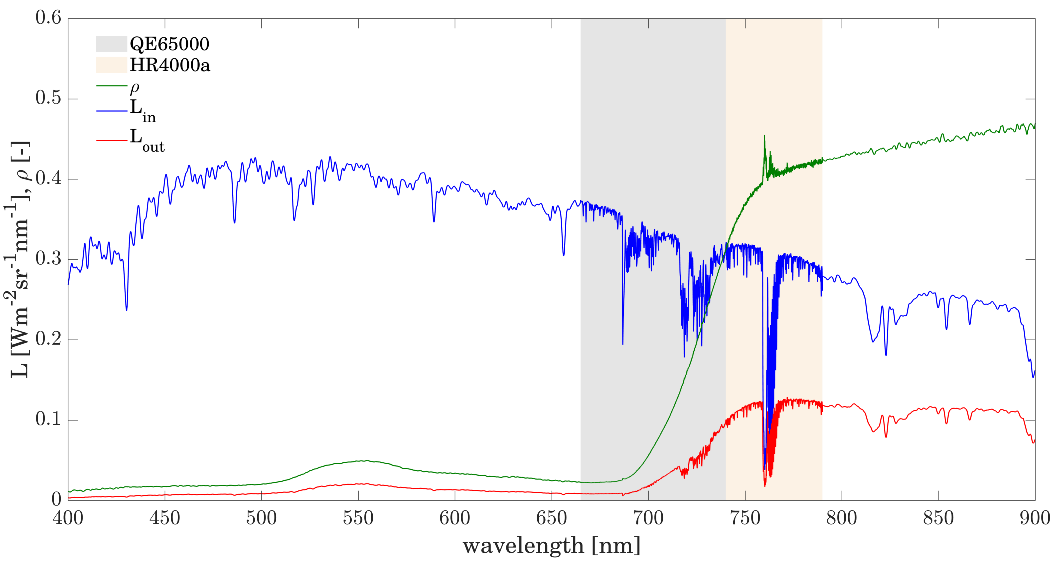

Figure 2: Example of the spectra collected with the three spectrometers merged together to obtain the highest resolution spectral configuration. The shaded area represents the regions where the data from the high resolution spectrometers (HR4000a and QE65000) were used instead of the full-range one (HR4000f).

2.2 Modeling setup

The radiative transfer modules of reflectance and fluorescence inside the leaf (Fluspect, [7]) and the canopy (RTMo and RTMf, respectively) of the SCOPE model version 1.70 (`https://github.com/Christiaanvandertol/SCOPE.git`; [2]) were coupled and inverted modifying an existing code by Dr. Ir. Christiaan van der Tol. Hereupon we refer to the coupled model as "RTMc". The inversion routine is based on a cost function that minimizes the differences between the measured and the modeled apparent reflectance. Several cost functions were tested before finding the right balance between stability of retrieved parameters and accuracy of modeled fluorescence values. The apparent reflectance (ρ_{app}) is a quantity defined by the ratio of the radiance leaving the vegetation surface and the incoming radiance. It differs from the true reflectance because of the addition of the emitted radiance (i.e. the fluorescence) to the reflected radiance (eq. 1). First, the components $\mathrm{L_{refl}}$ and F are modeled with the model RTMc from an arbitrary set of starting parameters (see Table 1 in [8] with the addition of the fqe parameter set to 0.01 and varying from 0 to 1) and the measured $\mathrm{L_{in}}$ spectrum. Then they were summed to obtain the modeled outgoing radiance and divided by the measured $\mathrm{L_{in}}$, to obtain a modeled spectrum of ρ_{app} at high resolution. The difference between measured and modeled ρ_{app} spectra is minimized through a numerical optimization algorithm based on MATLAB® `lsqnonlin` function, optimizing at the same time all the input parameters of the RTMc model. The output of this process is an optimized set of parameters, as well as the correspondent modeled spectra. Fqe is the model parameter for Φ_F, and the latter is used for both in this document.

Figure 3 shows an example of the true (ρ^{RTM}) and apparent (ρ^{RTM}_{app}) reflectance and fluorescence (F^{RTM}) spectra, simulated with the RTMc model.

RTMc needs as input the direct and diffuse component of the incoming light. Since this information was not measured in the field, we decomposed the measured total incoming radiance in its direct and diffuse components using FLEX-S3 standard atmosphere simulation produced with the MODTRAN® computer code, so that the sum of the resulting components equals the measured total $\mathrm{L_{in}}$. The obtained radiance fluxes were converted to irradiance (E) with a factor π (Figure 4).

$$\rho_{app} = \frac{L_{refl} + F}{L_{in}} = \frac{L_{out}}{L_{in}} \tag{1}$$

3 Results

In this section the preliminary results obtained during this STSM will be summarized .

3.1 Ground measurements

Results based on ground measurements show that both $\mathrm{F_{687}}$ and $\mathrm{F_{760}}$ quickly respond to the locking of the electron transport chain induced by the Dicuran (Figures 5, 6) while traditional reflectance based indices related to vegetation greenness as the MTCI ([9]) do not show any significant variation the first day after the treatment (Figure 7), when F have already reached high values. Moreover, F values of the plots treated with different doses of Dicuran seem to

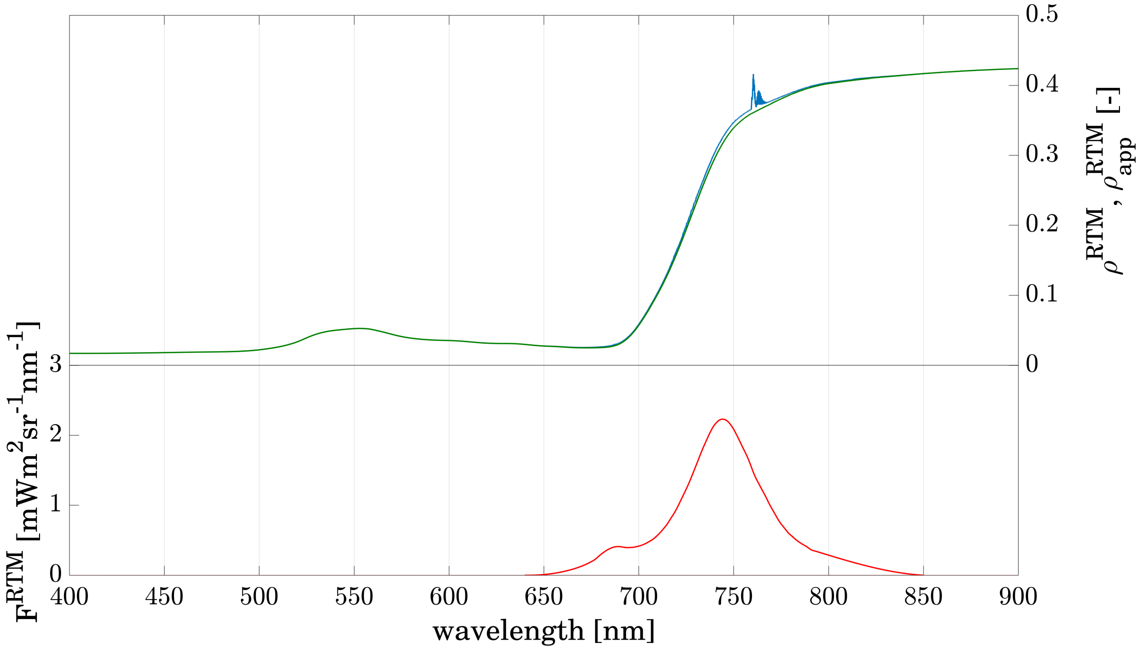

Figure 3: Example of the true (ρ^{RTM}) and apparent (ρ_{app}^{RTM}) reflectance and fluorescence (F^{RTM}) spectra, simulated with the RTMc model.

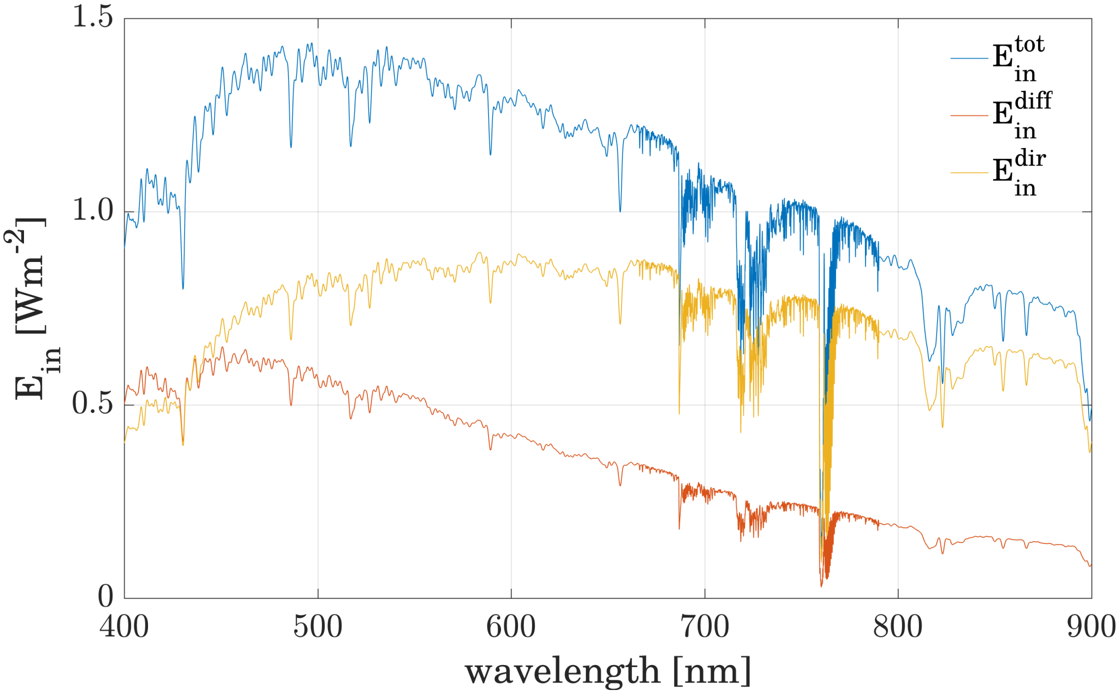

Figure 4: Example of the measured total irradiance (E_{in}^{tot}) and the decomposed direct (E_{in}^{dir}) and diffuse (E_{in}^{diff}) fluxes.

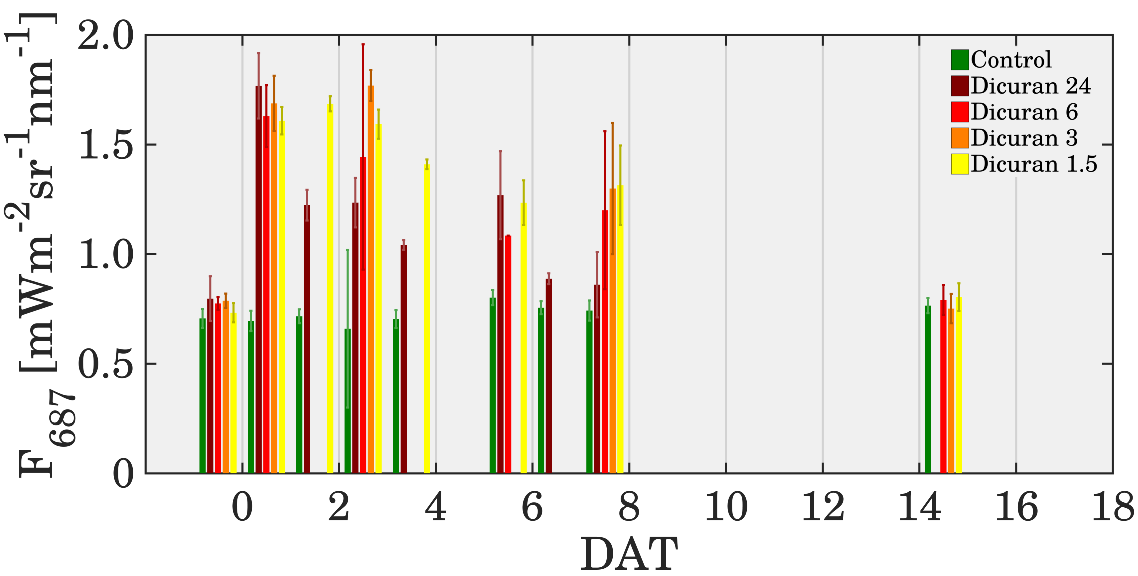

Figure 5: Time series of average F_{687} values for every plot, retrieved with SFM from ground measurements. The x axis shows the Day After Treatment (DAT), error bars are the standard deviation.

follow different temporal trends. The highest dose (plot 10,"Dicuran 24") causes an increase of $F_{760}$from 2 to 5.5 $mWm^{-2}sr^{-1}nm^{-1}$ in less than three hours, then the F value decreases steeply in the following days. F decline occurs together with a decrease in chlorophyll content. The lower doses (plots 3, 5, 4 and 7, "Dicuran 6", "Dicuran 3" and "Dicuran 1.5") cause a slower increase of F values: The maximum value (around 5 $mWm^{-2}sr^{-1}nm^{-1}$) is reached three days after the application, then the F values start to decrease gradually.

3.2 Model inversion

Figure 8 shows an example of the measured and retrieved apparent reflectance (top left) and fluorescence (top right) spectra. The region around the O_2-B and O_2-A oxygen absorption bands are highlighted. In the lower panels the relative root mean square error (RRMSE) for the reflectance, and the root mean square error (RMSE) for the F_{687} and F_{760} fluorescence retrieved with SFM are shown. The RRMSE between measured and modeled apparent reflectance is high in the blue region, it stays below 10% in the rest of the visible region, and drops below 5% for the far-red and near infrared regions. Figure 9 shows the deviation (difference) and the RRMSE between measured and retrieved apparent reflectance, computed for the whole dataset. The model sistematically overestimates the apparent reflectance in the blue region and is not perfectly able to reproduce the slope of the near infrared plateau, overestimating ρ_{app} between 800 and 850 nm and underestimating it afterwards. These discrepancies are somewhat minor, and can be attributed to the absorption spectra used as input in Fluspect or to an inaccurate modelling of the direct-diffuse components of the incoming radiation. These results, in fact, originates from measurements taken at different time of the day and in slightly different atmospheric conditions (although always cloud-

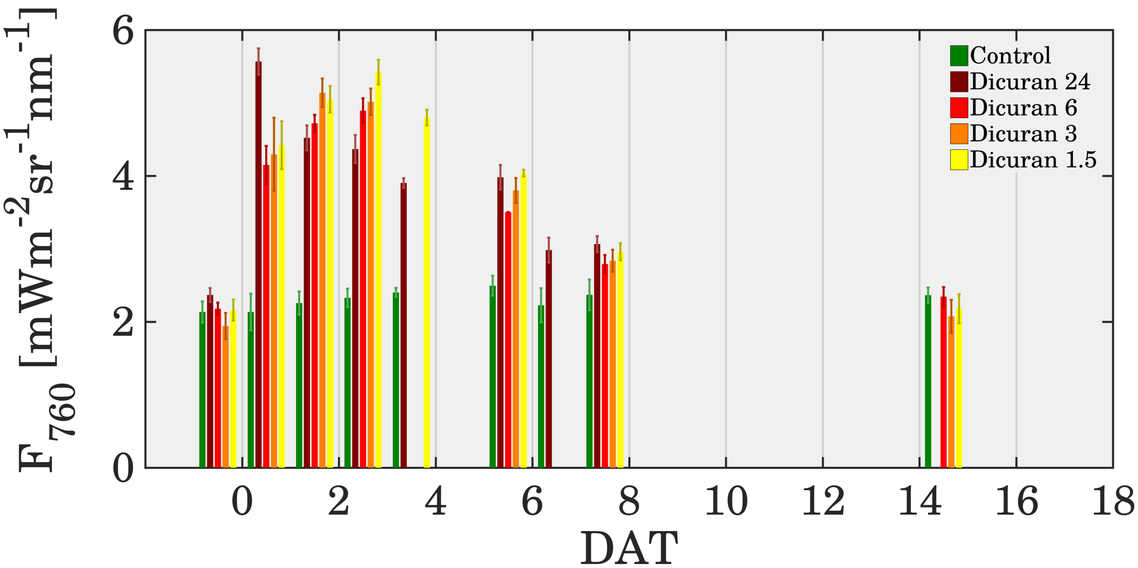

Figure 6: Time series of average F_{760} values for every plot, retrieved with SFM from ground measurements. The x axis shows the Day After Treatment (DAT), error bars are the standard deviation.

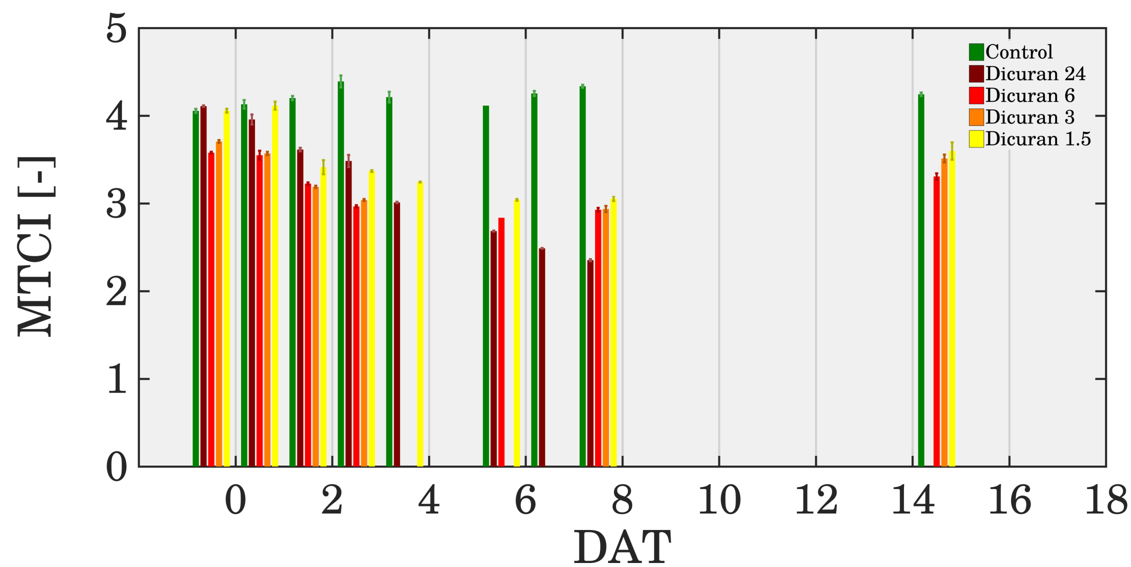

Figure 7: Time series of average MTCI values for every plot, calculated from ground measurements. The x axis shows the Day After Treatment (DAT), error bars are the standard deviation.

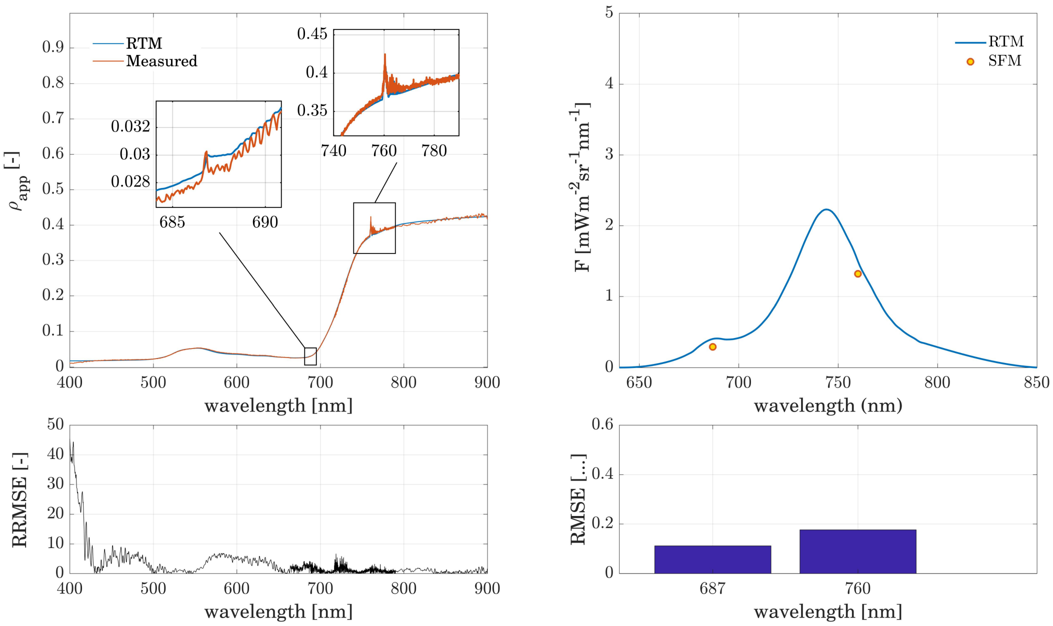

Figure 8: Example of the measured and retrieved apparent reflectance (top left) and fluorescence (top right) spectra. The region around the O_2-A and O_2-B oxygen absorption bands are highlighted. In the lower panels the relative root mean square error (RRMSE) for the reflectance, and the root mean square error (RMSE) for the F_{760} and F_{687} fluorescence ($mWm^{-2}sr^{-1}nm^{-1}$) are shown.

free), but the direct/diffuse ratio was fixed for every simulation. This last factor can be even more relevant to explain the residual difference in the modelling of the O_2-A band (750-770 nm). In fact the relative depth of the absorption band depends on the direct/diffuse ratio, and the lack of such a variable parametrization in the model can be a source of systematic error in the RTMC-based fluorescence retrieval. This happens also in the O_2-B band, but its depth and width are lower compared to the O_2-A band. Although this potential issue, F values at 687nm and 760nm retrieved with the RTMc inversion are similar to those retrieved with the SFM algorithms. The RMSE between the two is low, and close to the foreseen limit of measurements accuracy ($\approx$0.2 $mWm^{-2}sr^{-1}nm^{-1}$) due to the signal to noise ratio of the spectrometers. This value is also the requirement for the uncertainty of several FLEX fluorescence products, and can be taken as a threshold of accepted error. It is worth noting that the two fluorescence retrievals are completely independent and uses different parametrization of both fluorescence and true reflectance.

Figure 11 shows the scatterplot between F_{687} fluorescence values obtained with RTMc inversion (x axis) and retrieved with SFM (y axis), computed for the whole dataset. The linear regression model shows a very good correlation between the two fluorescence retrievals (R^2 = 0.78) and an average RMSE of 0.22 $mWm^{-2}sr^{-1}nm^{-1}$. As already pointed out, the RMSE around 0.2 $mWm^{-2}sr^{-1}nm^{-1}$ is reasonably good, especially considering that the observed range of variation of F_{687} is quite high. Two almost separate point clouds are clearly

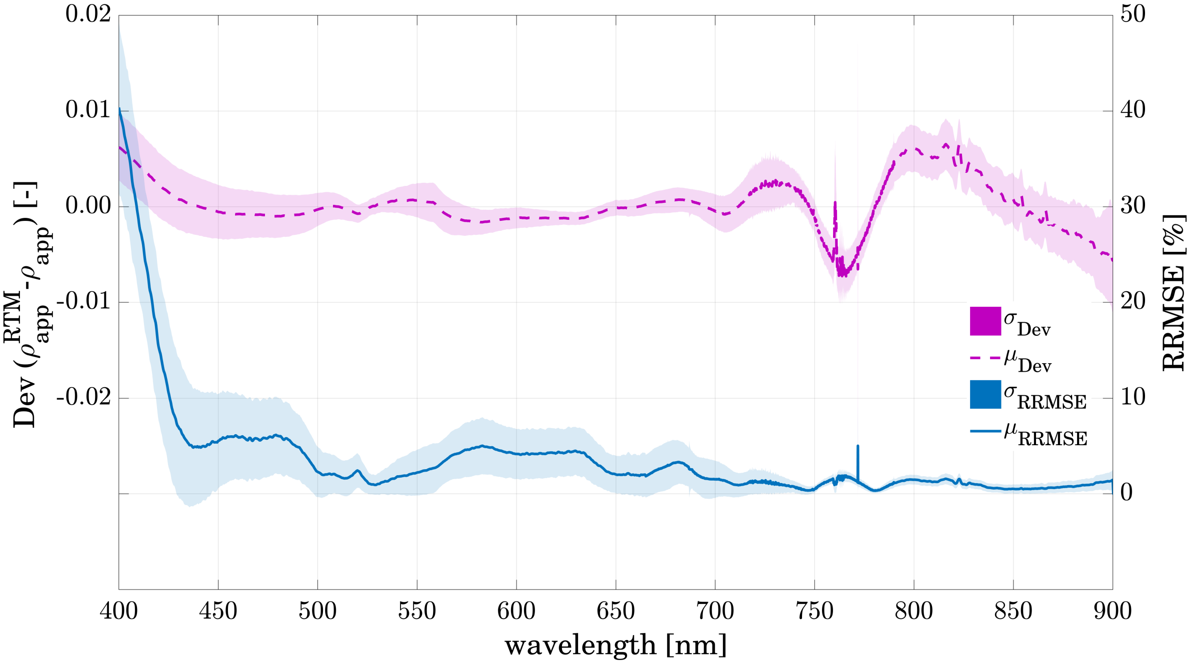

Figure 9: Deviation (solid blue line is the mean, shaded blue area is the standard deviation) and RRMSE (dashed purple line is the mean, purple area is the standard deviation) between measured and retrieved apparent reflectance.

distinguishable, one composed by F values between 0.5 and 1 mWm^{-2}sr^{-1}nm^{-1}, and the other composed by higher values.

Similar considerations can be done for F_{760} too (Figure 10), that shows a even higher R^2 (0.96) and a slope much closer to 1 (0.91), while the average RMSE is 0.23 mWm^{-2}sr^{-1}nm^{-1}. Thanks to the herbicide application, the range of variation of F_{760} is extreme if compared with what has been observed with the same measurement setup over a wide range of crops and natural vegetation ([4]), and the achieved agreement is therefore even more valuable.

3.3 Time series of retrieved parameters

Figure 12 shows the temporal variation of a selection of the parameters retrieved from the RTMc inversion for a control and a treated plot ("Dicuran 1.5"). The relative variation of leaf chlorophyll content is in line with the variation found in MTCI (Figure 7) and the laboratory pigment's extraction (data not shown). LAI values are pretty stable over time (as foreseen considering that no structural variation was expected or observed within the campaign time frame) and their slight increase over time in the control plot can be a compensating effect of the slight correspondent decrease in the retrieved Cab values. Fluorescence modelled values follow quite well the trends observed with SFM retrieval, including the abrupt increase after the treatment, showing the same underestimation (overestimation) for the red (far-red) fluorescence observed in Figure 11 (Figure 10) compared to SFM. Φ_F follows consistently the dynamics of F values, moreover its range of variation is quite high and inside the theoretical maximum range derived from an independent biophysical model [8]. According to

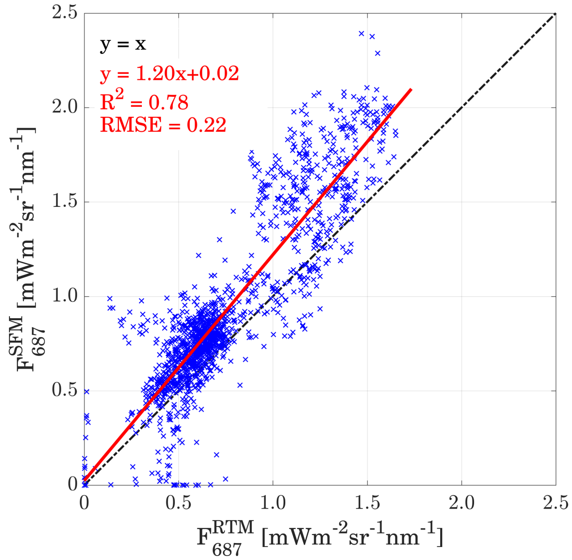

Figure 10: Scatterplot between F_{760} fluorescence values obtained with RTMc inversion (x axis) and retrieved with SFM (y axis). R^2 is the coefficient of determination for the linear regression model, RMSE is the root mean square error ($mWm^{-2}sr^{-1}nm^{-1}$).

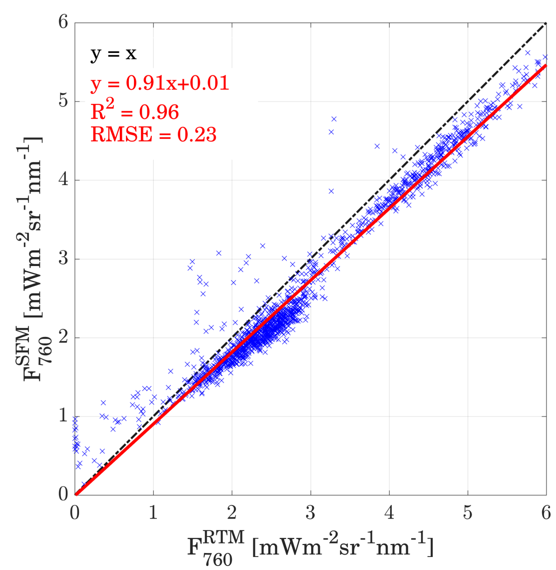

Figure 11: Scatterplot between F_{687} fluorescence values obtained with RTMc inversion (x axis) and retrieved with SFM (y axis). R^2 is the coefficient of determination for the linear regression model, RMSE is the root mean square error ($mWm^{-2}sr^{-1}nm^{-1}$).

the mathematical formulation of this model, in fact, Φ_F can be expressed as a ratio of rate coefficients:

$$\Phi_F = \frac{K_F}{K_P + K_N + K_D + K_F} \tag{2}$$

whit $K_F = 0.05$ and $K_D = 0.95$. Φ_F is maximum when both K_P and K_N are 0 (i.e. both PQ and NPQ are blocked), so that $\Phi_F^{max} = 0.05/1 = 0.05$, and minimum when K_P and K_N assumes very high values (e.g. 4), so that $\Phi_F^{min} = 0.05/9 \approx 0.005$ (both extremes are very unlikely). With unstressed (control) values around 0.010-0.015 and maximum stressed (treated) values around 0.030-0.035, the Φ_F values retrieved from the apparent reflectance through RTMc inversion are likely to be realistic, especially considering that the Chlorotoluron is known to strongly inhibit both PQ and NPQ. As a test, if we substitute $K_P = 0.02$ and $K_N = 0.02$ in equation 2, the resulting Φ_F value of 0.035 indicates that even a small amount of residual (non inhibited) PQ and NPQ would be enough to justify the retrieved maximum values.

4 Future collaboration with the host institution

Future collaboration with the host institution are foreseen to improve the obtained results and work towards further modelling of photosynthetic activity. Moreover, future collaboration is foreseen to asses the potential of enlarging the analysis to additional TOC hyperspectral datasets collected during the last 15 years by the Remote Sensing of Environmental Dynamics Laboratory (LTDA).

5 Foreseen publications/articles resulting from the STSM

Preliminary results of the work carried out during this STSM were shown at the EARSeL workshop, held in Zuerich (CH) in April 2017. Moreover, a peer-reviewed publication discussing the obtained and foreseen results is planned (target journal: Remote Sensing of Environment).

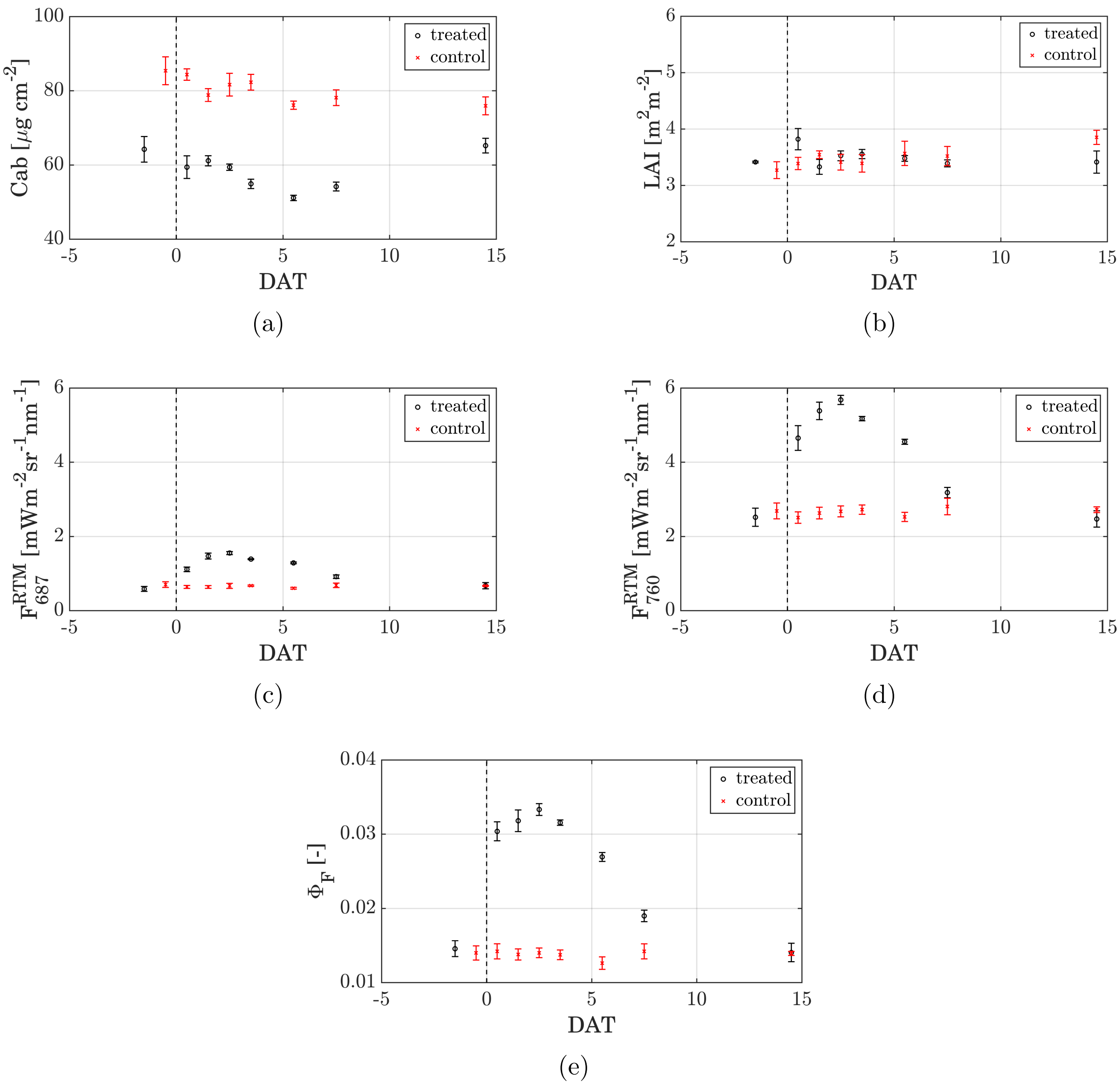

Figure 12: Time series of parameters retrieved from RTMc inversion. The x axis shows the Day After Treatment (DAT), error bars are the standard deviation.

References

[1] J. Verrelst, J. P. Rivera, C. van der Tol, F. Magnani, G. Mohammed, and J. Moreno, “Global sensitivity analysis of the SCOPE model: What drives simulated canopy-leaving sun-induced fluorescence?,” *Remote Sensing of Environment*, vol. 166, pp. 8–21, 2015.

[2] C. van der Tol, W. Verhoef, J. Timmermans, a. Verhoef, and Z. Su, “An integrated model of soil-canopy spectral radiances, photosynthesis, fluorescence, temperature and energy balance,” *Biogeosciences*, vol. 6, no. 12, pp. 3109–3129, 2009.

[3] S. Cogliati, W. Verhoef, S. Kraft, N. Sabater, L. Alonso, J. Vicent, J. Moreno, M. Drusch, and R. Colombo, “Retrieval of sun-induced fluorescence using advanced spectral fitting methods,” *Remote Sensing of Environment*, vol. 169, pp. 344–357, 2015.

[4] M. Rossini, M. Meroni, M. Celesti, S. Cogliati, T. Julitta, C. Panigada, U. Rascher, C. van der Tol, and R. Colombo, “Analysis of Red and Far-Red Sun-Induced Chlorophyll Fluorescence and Their Ratio in Different Canopies Based on Observed and Modeled Data,” *Remote Sensing*, vol. 8, no. 5, p. 412, 2016.

[5] M. Meroni and R. Colombo, “3S: A novel program for field spectroscopy,” *Computers & Geosciences*, vol. 35, pp. 1491–1496, 7 2009.

[6] M. Meroni, A. Barducci, S. Cogliati, F. Castagnoli, M. Rossini, L. Busetto, M. Migliavacca, E. Cremonese, M. Galvagno, R. Colombo, and U. M. Di Cella, “The hyperspectral irradiometer, a new instrument for long-term and unattended field spectroscopy measurements,” *Review of Scientific Instruments*, vol. 82, no. 4, pp. 1–10, 2011.

[7] N. Vilfan, C. van der Tol, O. Muller, U. Rascher, and W. Verhoef, “Fluspect-B: A model for leaf fluorescence, reflectance and transmittancespectra,” *Remote Sensing of Environment*, vol. 186, pp. 596–615, 2016.

[8] C. van der Tol, M. Rossini, U. Rascher, W. Verhoef, and G. Mohammed, “A model and measurement comparison of diurnal cycles of sun induced chlorophyll fluorescence of crops,” *Remote Sensing of Environment*, vol. 186, no. iii, pp. 1–13, 2016.

[9] J. Dash and P. J. Curran, “The MERIS terrestrial chlorophyll index,” *International Journal of Remote Sensing*, vol. 25, no. 23, pp. 5403–5413, 2004.